CALIBRATION OF NaI (Tl) CYLINDRICAL DETECTOR USING AXIALLY SHIFTED RADIOACTIVE CYLINDRICAL SOURCES

by

Mona M. GOUDA

Physics Department, Faculty of Science, Alexandria University, Alexandria, Egypt

Scientific paper
https://doi.org/10.2298/NTRP190708035G

In this article, the full energy peak efficiency of NaI detector using non-axial cylindrical sources is calculated by using a new efficient theoretical approach. This approach depends on using the efficiency transfer method and analytical calculations of the average path length of a gamma photon inside the source to the detector system. Measured efficiencies made by using ^{152}Eu aqueous radioactive cylindrical sources with volumes 25 ml and 400 ml. Comparing calculated efficiencies to the measured one showed good agreement enabling the validation of this approach.

Key words: full energy peak efficiency, cylindrical source, average path length, effective solid angle ratio, efficiency transfer method

INTRODUCTION

Inorganic Scintillation detector is used in gamma spectrometers due to its availability in massive size and low cost. The most widely used is NaI (Tl) scintillator as a result of its low price, high light yield, high density and mature producing technique [1]. Since radionuclide activity concentrations in the environmental samples are very low; so NaI (Tl) detectors are used according to its high efficiency [2]. For analysis of environmental samples or nuclear waste, the detector must be calibrated by using standard sources. Since it is not practical to prepare standard sources that match the nuclear and physical properties of each waste or environmental sample [3], different techniques were introduced to complete calibration [4-9]. The efficiency transfer method is one of the most useful techniques for calculation of the full energy peak efficiency of the detectors. This method is applied for different geometrical shapes and is derived from the known efficiency for reference source-detector geometry [10-13]. Moreover, some theoretical methods were used for the average path length in the efficiency and correction factor calculations [14, 15]. Recently co-workers used the new theoretical approach to calculate the full energy peak efficiency of cylindrical detector using co-axial cylindrical sources with different volumes and placed on the end cap of the detector [16, 17]. This approach combined between efficiency transfer method and analytical calculations of the average path length of the gamma photon inside the source to the detector system. In this paper, the previous approach is used to calculate the full energy peak efficiency of NaI (Tl) cylindrical detector using cylindrical sources axially shifted *vs*. the detector.

By using the efficiency transfer method, the full energy peak efficiency of the cylindrical detector using axially shifted radioactive cylindrical source was calculated as follows

$$\varepsilon_{(\text{cylinder})} \quad \frac{\Omega_{\text{eff(cylinder)}}}{\Omega_{\text{eff(point)}}} \varepsilon_{(\text{point})} \tag{1}$$

where $\varepsilon_{(\text{cylinder})}$ is the calculated full energy peak efficiency of the detector using cylindrical sources axially shifted. $\varepsilon_{(\text{point})}$ – the experimental full energy peak efficiency of the detector using an axial radioactive point source as a reference geometry while, $\Omega_{\text{eff(cylinder)}}$ and $\Omega_{\text{eff(point)}}$, are the effective solid angles subtended by the detector surface with the radioactive cylindrical source and the reference geometry (axial point source), respectively. The values of the effective solid angle depend on the geometrical shape of the source and the detector, the position of the source with respect to the detector and the values of polar θ and azimuthal φ angles. The calculation of $\Omega_{\text{eff(point)}}$ for axial point source done in the previous work [16], so in the next section we focus on the calculation of $\Omega_{\text{eff(cylinder)}}$ for cylindrical sources axially shifted *vs*. the detector.

* Corresponding author; e-mail: ahec3@yahoo.com

MATHEMATICAL MODEL

Non-axial point source at a height smaller than or equal to the detector length from the detector base ($h \quad L$)

Consider a non – axial point source placed at lateral distance ρ ($\rho > R$) from the axis of cylindrical (2R $\times$ L) detector and at height h ($h \quad L$) from the detector base as seen in fig. 1.

In this case, there are four different polar angles appear as follows:

– θ_{Emin} and θ_{EXmin} are the minimum polar angles in which the photon enters from the detector base and the detector face respectively and are given by

$$\theta_{\text{E min}} \quad \tan^{1} \frac{\rho\cos\varphi \quad \sqrt{R^2 \quad \rho^2 \sin^2\varphi}}{h}$$

$$\theta_{\text{EX min}} \quad \pi \quad \tan^{1} \frac{\rho\cos\varphi \quad \sqrt{R^2 \quad \rho^2 \sin^2\varphi}}{L \quad h} \qquad (2)$$

– θ_{Emax} and θ_{EXmax} are the maximum polar angles in which the photon exits from the detector base and the detector face respectively and are given by

$$\theta_{\text{Emax}} \quad \tan^{1} \frac{\rho\cos\varphi \quad \sqrt{R^2 \quad \rho^2 \sin^2\varphi}}{h}$$

$$\theta_{\text{EX max}} \quad \pi \quad \tan^{1} \frac{\rho\cos\varphi \quad \sqrt{R^2 \quad \rho^2 \sin^2\varphi}}{L \quad h} \qquad (3)$$

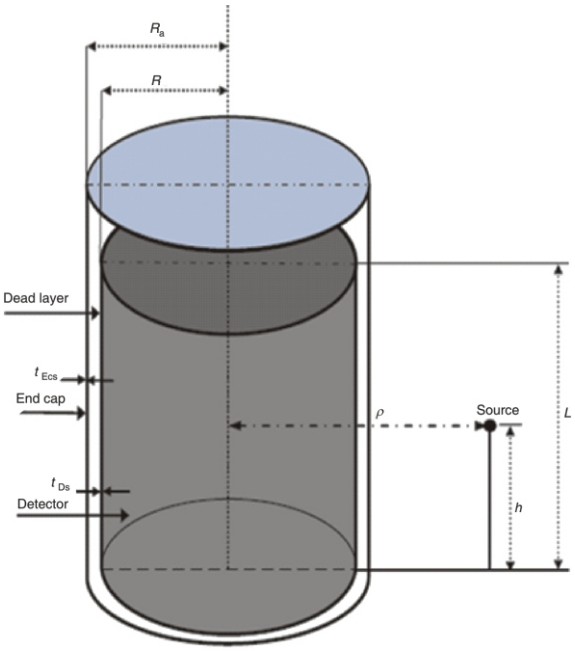

Figure 1. A cylindrical detector with a non-axial point source at a position lower than the detector surface

The maximum azimuthal angle for the photon to enter the detector from the side is represented by

$$\varphi_c \quad \sin^{1} \frac{R}{\rho} \qquad (4)$$

There are three main cases to be considered for the photon emitted from the isotropic radiating point source. The photon enters from the side of the detector and may get out from its base (d_1), side (d_2) or face (d_3) as shown in figs. 2 and 3. The distances traveled by the

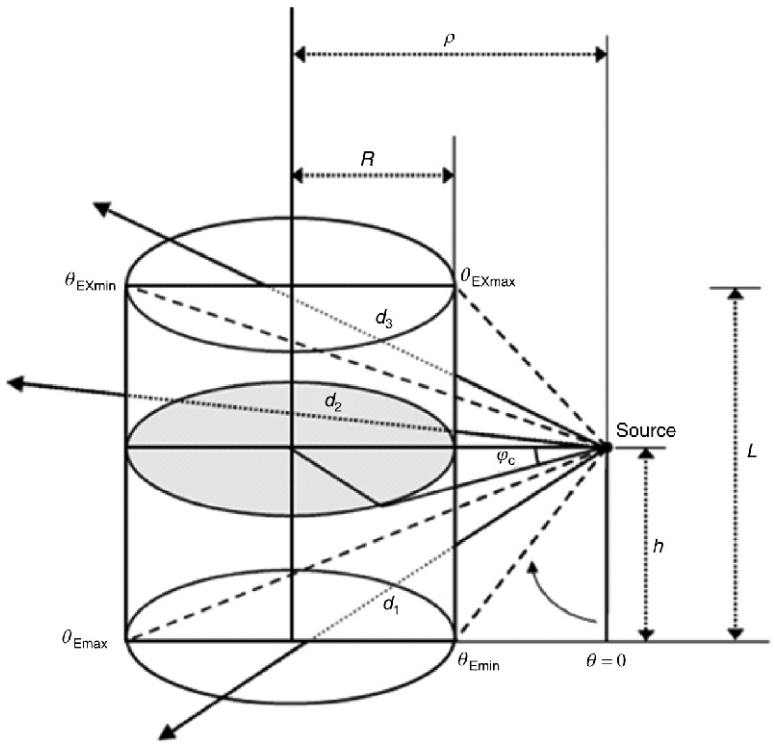

Figure 2. Non-axial point source ($h < L$)

Figure 3. Non-axial point source ($h = L$)

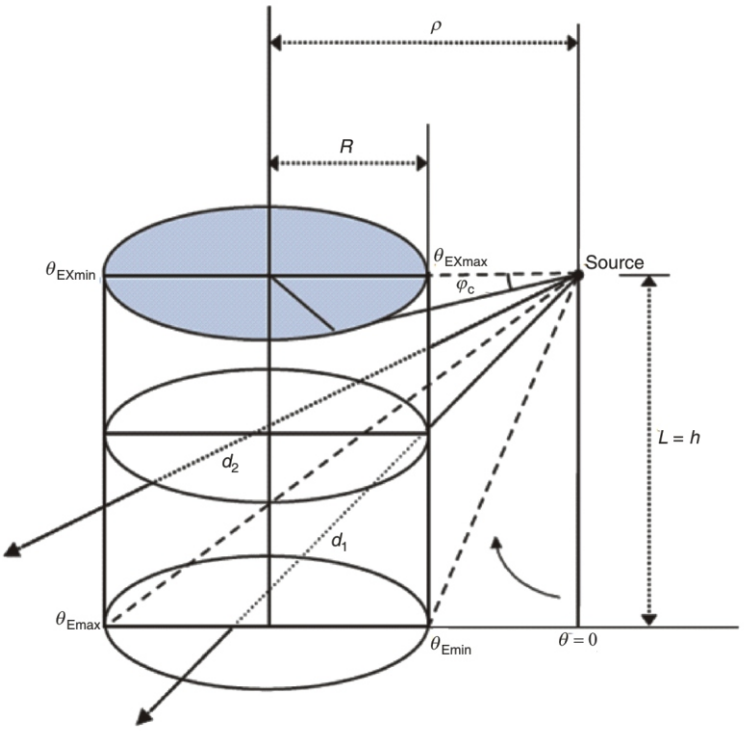

photon in all cases are given by the following equations

$$d_1 \quad \frac{h}{\cos\theta} \quad \frac{\rho\cos\varphi \quad \sqrt{R^2 \quad \rho^2\sin^2\varphi}}{\sin\theta} \tag{5}$$

$$d_2 \quad \frac{2\sqrt{R^2 \quad \rho^2\sin^2\varphi}}{\sin\theta} \tag{6}$$

$$d_3 \quad \frac{L \quad h}{\left|\cos(\pi \quad \theta)\right|} \quad \frac{\rho\cos\varphi \quad \sqrt{R^2 \quad \rho^2\sin^2\varphi}}{\left|\sin(\pi \quad \theta)\right|} \tag{7}$$

According to the geometry of figs. 2 and 3, the average path length $\bar{d}$ traveled by the photon through the detector is given by

$$\bar{d} \quad \frac{I}{\int_0^{\varphi_c}\int_{\theta_{Emin}}^{\theta_{EXmax}} \sin\theta\,\mathrm{d}\theta\,\mathrm{d}\varphi} \tag{8}$$

where I has different values according to the values of the polar angles, as follows

If $\theta_{Emin} \quad \theta_{Emax} \quad \theta_{EXmin} \quad \theta_{EXmax}$ and $h < L$ then I is given by

$$I \quad \int_0^{\varphi_c}\left[\int_{\theta_{Emin}}^{\theta_{Emax}} d_1\sin\theta\,\mathrm{d}\theta \quad \int_{\theta_{Emax}}^{\theta_{EXmin}} d_2\sin\theta d\theta + \int_{\theta_{EXmin}}^{\theta_{EXmax}} d_3\sin\theta\,\mathrm{d}\theta\right]\mathrm{d}\varphi \tag{9}$$

If $\theta_{Emin} \quad \theta_{Emax} \quad (\theta_{EXmin} \quad \theta_{EXmax})$ and $h = L$ then I is given by

$$I \quad \int_0^{\varphi_c}\left[\int_{\theta_{Emin}}^{\theta_{Emax}} d_1\sin\theta\,\mathrm{d}\theta \quad \int_{\theta_{EXmax}}^{\theta_{EXmax}} d_2\sin\theta\mathrm{d}\theta\right]\mathrm{d}\varphi \tag{10}$$

Since the cylindrical source axially shifted *vs.* the detector and at height smaller than or equal to the detector length from the detector base ($h \quad L$), the attenuation in the dead layer and end cap will be from the side surface of them not from the upper surface. Table 1 shows the values of the average path length and the possible path lengths traveled by the photon through the dead layer and end cap. Where the detector has a

Table 1. Values of the possible path lengths and the average path length travelled by the photon through the dead layer and end cap

Items	Dead layer	End cap
The possible path lengths	$t_d \quad \frac{\sqrt{(R \quad t_{Ds})^2 \quad \rho^2\sin^2\varphi} \quad \sqrt{R^2 \quad \rho^2\sin^2\varphi}}{\sin\theta}$	$t_{Ec} \quad \frac{\sqrt{(R_a \quad t_{Ecs})^2 \quad \rho^2\sin^2\varphi} \quad \sqrt{R_a^2 \quad \rho^2\sin^2\varphi}}{\sin\theta}$
The average path length	$\bar{\delta}_{Dlay} \quad \frac{\int_0^{\varphi_c}\int_{\theta_{Emin}}^{\theta_{EXmax}} t_d\sin\theta\mathrm{d}\theta\mathrm{d}\varphi}{\int_0^{\varphi_c}\int_{\theta_{Emin}}^{\theta_{EXmax}} \sin\theta\mathrm{d}\theta\mathrm{d}\varphi}$	$\bar{\delta}_{Ecap} \quad \frac{\int_0^{\varphi_c}\int_{\theta_{Emin}}^{\theta_{EXmax}} t_{Ec}\sin\theta\mathrm{d}\theta\mathrm{d}\varphi}{\int_0^{\varphi_c}\int_{\theta_{Emin}}^{\theta_{EXmax}} \sin\theta\mathrm{d}\theta\mathrm{d}\varphi}$

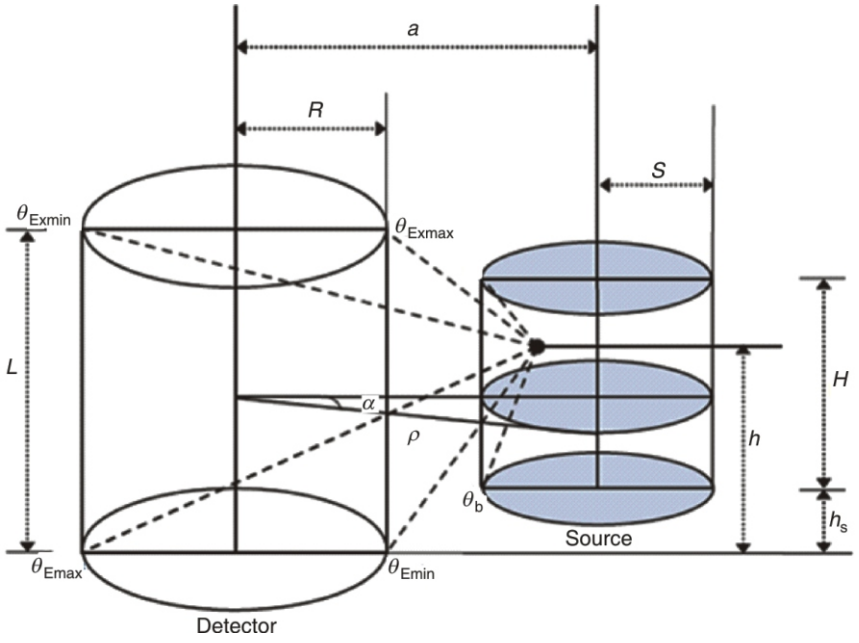

Figure 4. Cylindrical source axially shifted *vs.* the detector with ($H + h_s$) *L*

dead layer covering its side surface with thickness t_{Ds}. Also, the thickness of the side surface of the detector end cap material and its inner radius is given by t_{Ecs} and R_a respectively.

Cylindrical source axially shifted *vs.* the detector

The effective solid angle $\Omega_{\text{eff(cylinder)}}$, of the cylindrical detector using a cylindrical source of height H and radius S, is given by

$$\Omega_{\text{eff(cylinder)}} \quad f_{\text{att}} S_{\text{self}} S_{\text{sc}} (1 \quad \text{e}^{\ \mu \bar{d}}) \Omega_{\text{pure(cylinder)}} \tag{11}$$

and

$$\Omega_{\text{pure (cylinder)}} \quad \frac{\int_{h_s}^{H} \int_{0}^{\rho_1} \int_{0}^{\theta_{\text{Emin}}} \int_{h_s}^{\alpha_1 \rho_2 \varphi_c \theta_{\text{EXmax}}} \sin\theta \rho \, \text{d}\theta \, \text{d}\varphi \, \text{d}\rho \, \text{d}\alpha \, \text{d}h}{\pi S^2 H} \tag{12}$$

where f_{att} is the attenuation factor of dead layer and end cap, S_{self} – the self-attenuation factor of the source matrix, S_{sc} – the attenuation factor of the container material, $\bar{d}$ – the average path length traveled by the photon through the detector, μ – the attenuation coefficient of the detector material, and $V = \ \text{S}^2\text{H}$ is the volume of the cylindrical source. Now $\bar{d}$ will has a new form due to the geometry of fig. 4.

$$\bar{d} \quad \frac{\int_{h_s}^{H} \int_{0}^{\rho_1} \int_{h_s}^{\alpha_1 \rho_2} I \rho \, \text{d}\rho \, \text{d}\alpha \, \text{d}h}{\int_{h_s}^{H} \int_{0}^{\rho_1} \int_{0}^{\theta_{\text{Emin}}} \int_{h_s}^{\alpha_1 \rho_2 \varphi_c \theta_{\text{EXmax}}} \sin\theta \rho \, \text{d}\theta \, \text{d}\varphi \, \text{d}\rho \, \text{d}\alpha \, \text{d}h} \tag{13}$$

where I is defined before in eqs. (9) and (10) while, the angle α_1 and the maximum displacement ρ_1 and ρ_2 can be given by

$$\alpha_1 \quad \sin^{\ 1} \frac{S}{a} \tag{14}$$

$$\begin{aligned} \rho_1 \quad & a\cos\alpha \quad \sqrt{S^2 \quad a^2 \sin^2 \alpha} \\ \rho_2 \quad & a\cos\alpha \quad \sqrt{S^2 \quad a^2 \sin^2 \alpha} \end{aligned} \tag{15}$$

The attenuation factor f_{att} is expressed as

$$f_{\text{att}} \quad \text{e}^{\ \mu_{\text{dlay}} \ \bar{\delta}_{\text{dlay}}} \ \text{e}^{\ \mu_{\text{ecap}} \ \bar{\delta}_{\text{ecap}}} \tag{16}$$

where μ_{dlay} and μ_{ecap} are the attenuation coefficients of the dead layer and end cap, respectively. The average path length traveled by the photon inside the detector dead layer $\bar{\delta}_{\text{dlay}}$ and the detector end cap material $\bar{\delta}_{\text{ecap}}$ is given by eqs. (17) and (18), respectively.

$$\bar{\delta}_{\text{dlay}} \quad \frac{\int_{h_s}^{H} \int_{0}^{\rho_1} \int_{0}^{\theta_{\text{Emin}}} \int_{h_s}^{\alpha_1 \rho_2 \varphi_c \theta_{\text{EXmax}}} t_{\text{d}} \sin\theta \rho \, \text{d}\theta \, \text{d}\varphi \, \text{d}\rho \, \text{d}\alpha \, \text{d}h}{\int_{h_s}^{H} \int_{0}^{\rho_1} \int_{0}^{\theta_{\text{Emin}}} \int_{h_s}^{\alpha_1 \rho_2 \varphi_c \theta_{\text{EXmax}}} \sin\theta \rho \, \text{d}\theta \, \text{d}\varphi \, \text{d}\rho \, \text{d}\alpha \, \text{d}h} \tag{17}$$

$$\bar{\delta}_{\text{ecap}} \quad \frac{\int_{h_s}^{H} \int_{0}^{\rho_1} \int_{0}^{\theta_{\text{Emin}}} \int_{h_s}^{\alpha_1 \rho_2 \varphi_c \theta_{\text{EXmax}}} t_{\text{ec}} \sin\theta \rho \, \text{d}\theta \, \text{d}\varphi \, \text{d}\rho \, \text{d}\alpha \, \text{d}h}{\int_{h_s}^{H} \int_{0}^{\rho_1} \int_{0}^{\theta_{\text{Emin}}} \int_{h_s}^{\alpha_1 \rho_2 \varphi_c \theta_{\text{EXmax}}} \sin\theta \rho \, \text{d}\theta \, \text{d}\varphi \, \text{d}\rho \, \text{d}\alpha \, \text{d}h} \tag{18}$$

where t_{d} and t_{ec} are defined before in tab. 1.

For the cylindrical source there are three paths for the photon to leave the source as follows:

To exit from the radioactive source base

$$t_{\text{b}} \quad \frac{h \quad h_{\text{s}}}{\cos\theta} \tag{19}$$

To exit from the radioactive source side

$$t_s \quad \frac{(\rho - a)\cos\varphi \quad \sqrt{S^2 \quad (\rho \quad a)^2 \sin^2\varphi}}{\sin\theta} \tag{20}$$

To exit from the radioactive source face

$$t_f \quad \frac{H \quad (h \quad h_s)}{\cos(\pi \quad \theta)} \tag{21}$$

According to fig. 4, there are two new polar angles appear which are θ_f (the maximum polar angle where the photon exit from the source face) and θ_b (the maximum polar angle where the photon exit from the source base) and they are given by the following equations

$$\theta_f \quad \pi \quad \tan^{1} \frac{(\rho \quad a)\cos\varphi \quad \sqrt{S^2 \quad (\rho \quad a)^2 \sin^2\varphi}}{H \quad (h \quad h_s)} \tag{22}$$

$$\theta_b \quad \tan^{1} \frac{(\rho \quad a)\cos\varphi \quad \sqrt{S^2 \quad (\rho \quad a)^2 \sin^2\varphi}}{(h \quad h_s)} \tag{23}$$

The self attenuation factor is represented by

$$S_{self} \quad e^{\mu_s \bar{t}_s} \tag{24}$$

where μ_s is the attenuation coefficient of the source matrix and $\bar{t}_s$ – the average path length traveled by a photon inside the source and is given by

$$\bar{t}_s \quad \frac{\int_{h_s}^{H} \int_{0}^{h_s \alpha_1 \rho_2} g_s \rho \, d\rho \, d\alpha \, dh}{\int_{h_s}^{H} \int_{0}^{h_s \alpha_1 \rho_2 \varphi_c \theta_{EXmax}} \sin\theta \rho \, d\rho \, d\alpha \, dh} \tag{25}$$

where g_s has different values according to the values of the polar angles θ_i as follows:

When $\theta_{Emin} < \theta_b < \theta_f < \theta_{EXmax}$

$$g_s \quad \int_{0}^{\varphi_c} \int_{\theta_{Emin}}^{\theta_b} t_b \int_{\theta_b}^{\theta_f} t_s \int_{\theta_f}^{\theta_{EXmax}} t_f \sin\theta \, d\theta \, d\varphi \tag{26}$$

When $\theta_b \quad \theta_{Emin} < \theta_f < \theta_{EXmax}$

$$g_s \quad \int_{0}^{\varphi_c} \int_{\theta_{Emin}}^{\theta_f} t_s \int_{\theta_f}^{\theta_{EXmax}} t_f \sin\theta \, d\theta \, d\varphi \tag{27}$$

When $\theta_{Emin} < \theta_b < \theta_{EXmax} \quad \theta_f$

$$g_s \quad \int_{0}^{\varphi_c} \int_{\theta_{Emin}}^{\theta_b} t_b \int_{\theta_b}^{\theta_{EXmax}} t_s \sin\theta \, d\theta \, d\varphi \tag{28}$$

When $\theta_b \quad \theta_{Emin} < \theta_{EXmax} \quad \theta_f$

$$g_s \quad \int_{0}^{\varphi_c} \int_{\theta_{Emin}}^{\theta_{EXmax}} t_s \sin\theta \, d\theta \, d\varphi \tag{29}$$

For the source container; If t_1, t_2, and t_3 are bottom, wall and face thickness of the source container respectively, so, the photon which is detected by the detector may be exited from the base, the side or from the face of the source container. The possible path lengths for three cases are given by eqs. (30)-(32), respectively.

$$t_{Scb} \quad \frac{t_1}{\cos\theta} \quad \text{(from base)} \tag{30}$$

$$\frac{t_{Scs}}{\sqrt{(S \quad t^2)^2 \quad (\rho \quad a)^2 \sin^2\varphi} \quad \sqrt{S^2 \quad (\rho \quad a)^2 \sin^2\varphi}} \quad \frac{\sin\theta}{\text{(from the side)}} \tag{31}$$

$$t_{Scf} \quad \frac{t_3}{\cos(\pi \quad \theta)} \text{(from face)} \tag{32}$$

The same as in the case of the source there are only two polar angles which are θ_{Scf} (the maximum polar angle where the photon exit from the source container face) and θ_{Scb} (the maximum polar angle where the photon exit from the source container base) and they are given by the following equations

$$\theta_{Scf} \quad \pi \quad \tan^{1} \frac{(\rho - a)\cos\varphi \quad \sqrt{(S \quad t_2)^2 \quad (\rho \quad a)^2 \sin^2\varphi}}{H \quad (h \quad h_s) \quad t_3} \tag{33}$$

$$\theta_{Scb} \quad \tan^{1} \frac{(\rho - a)\cos\varphi \quad \sqrt{(S \quad t_2)^2 \quad (\rho \quad a)^2 \sin^2\varphi}}{(h \quad h_s) \quad t_1} \tag{34}$$

The attenuation factor of the container material is represented by

$$S_{sc} \quad e^{\mu_c \bar{t}_{sc}} \tag{35}$$

where μ_c is the attenuation coefficient of the source container material and $\bar{t}_{sc}$ – the average path length traveled by a photon through the source container and is given by

$$\bar{t}_{sc} \quad \frac{\int_{h_s}^{H} \int_{0}^{h_s \alpha_1 \rho_2} g_{sc} \rho \, d\rho \, d\alpha \, dh}{\int_{h_s}^{H} \int_{0}^{h_s \alpha_1 \rho_2 \varphi_c \theta_{EXmax}} \sin\theta \rho \, d\rho \, d\alpha \, dh} \tag{36}$$

where g_{sc} has different values according to the values of the polar angles θ_i as follows:

When $\theta_{Emin} < \theta_{Scb} < \theta_{Scf} < \theta_{EXmax}$

$$g_{sc} \quad \int_{0}^{\varphi_c} \int_{\theta_{Emin}}^{\theta_{Scb}} t_{Scb} \int_{\theta_{Scb}}^{\theta_{Scf}} t_{Scs} \int_{\theta_{Scf}}^{\theta_{EXmax}} t_{Scf} \sin\theta \, d\theta \, d\varphi \tag{37}$$

When $\theta_{Scb} \quad \theta_{Emin} < \theta_{Scf} < \theta_{EXmax}$

$$g_{sc} \quad \int_{0}^{\varphi_c} \int_{\theta_{Emin}}^{\theta_{Scf}} t_{Scs} \int_{\theta_{Scf}}^{\theta_{EXmax}} t_{Scf} \sin\theta \, d\theta \, d\varphi \tag{38}$$

When $\theta_{Emin} < \theta_{Scb} < \theta_{EXmax} \quad \theta_{Scf}$

$$g_{sc} \quad \int_{0}^{\varphi_c} \int_{\theta_{Emin}}^{\theta_{Scb}} t_{Scb} \int_{\theta_{Scb}}^{\theta_{EXmax}} t_{Scs} \sin\theta \, d\theta \, d\varphi \tag{39}$$

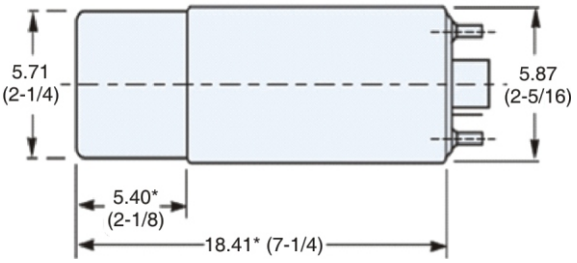

Figure 5. The manufactory drawing of NaI (Tl) detector, dimensions in cm (inch)

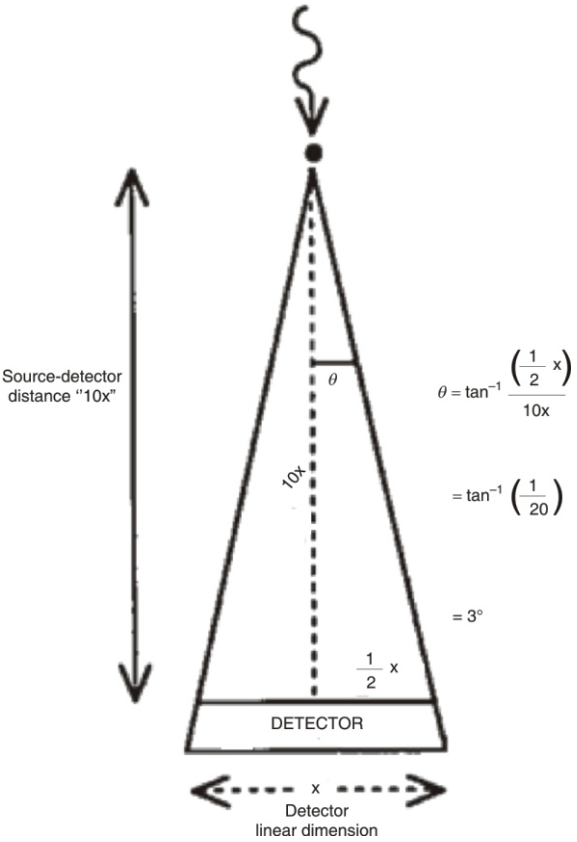

Figure 6. Narrow beam according to Hendee *et al*., [18]

When $\theta_{Scb} \quad \theta_{Emin} < \theta_{EXmax} \quad \theta_{Scf}$

$$g_{sc} \quad \int_{0}^{\varphi_c} \int_{\theta_{Emin}}^{\theta_{EXmax}} t_{Scs} \sin\theta \, d\theta \, d\varphi \qquad (40)$$

EXPERIMENT SET-UP

The detector used in these measurements was the NaI (Tl) detector (model 802-2x2 in, Canberra) with resolution 8.5 % at the 662 keV peak of ^{137}Cs. The manufactory drawing of the NaI (Tl) detector is illustrated in fig. 5.

The radioactive point sources (reference) ^{241}Am, ^{133}Ba, ^{152}Eu, ^{137}Cs were used in these measurements with an energy range from 59.52 keV to 1408 keV [17]. There is no collimator used in the present arrangement, so according to Hendee *et al*., [18] the beam of photons must be narrow beam and that is happening when the source-detector distance equals ten times the diameter of the detector as shown in fig. 6. According to that, all point sources are located at an axial distance equal to 50 cm from the detector cap. The radioactive cylindrical sources are polypropylene (PP) plastic vials of volumes V1 = 25 ml (outer diameter = 3.21cm, height = 3.621 cm, wall thickness = = 0.12cm) and V2 = 400 ml (outer diameter =11.389 cm, height = 4.225 cm, wall thickness = 0.203cm) full of a solution containing ^{152}Eu radionuclide that emits γ-ray within the energy vary from 121 keV to 1408 keV. The activity of the sources is (5048 49.98 Bq). The cylindrical sources positioned with axial shift *vs*. the detector. The distance (a) between the axis of the sources V1 and V2 and that of the detector are 4.47 cm and 8.55 cm respectively.

EXPERIMENTAL EFFICIENCIES

By knowing the area of full energy peak, the experimental full energy peak efficiency is obtained by

$$\varepsilon(E) \quad \frac{N(E)}{TA_s P(E) e^{\lambda \Delta T}} \qquad (41)$$

where $N(E)$ is the number of counts in the full-energy peak and it can be obtained using Genie 2000 software, $P(E)$ – the photon emission probability at energy E, λ – the decay constant, A_S – the radionuclide activity, T [s] – the measuring time, and T – the time interval over which the source decays corresponding to the run time. The uncertainty in the full energy peak efficiency σ_ε is given by

$$\sigma_\varepsilon \quad \varepsilon \sqrt{\left(\frac{\partial \varepsilon}{\partial A}\right)^2 \sigma_\varepsilon^2 \quad \left(\frac{\partial \varepsilon}{\partial P}\right) \sigma_P^2 \quad \left(\frac{\partial \varepsilon}{\partial N}\right) \sigma_N^2} \qquad (42)$$

where σ_A, σ_P, and σ_N, are the uncertainties associated with the quantities A_S, $P(E)$, and $N(E)$, respectively.

RESULTS AND DISCUSSION

The efficiency transfer method used to convert the full energy peak efficiency curve for using axis radioactive point sources measured at a distance 50 cm from the detector cap to the full energy peak efficiency using radioactive cylindrical sources positioned axial shift *vs*. of the detector and $(H + hs)$ L. These calculations are done for 2 2 in cylindrical NaI (Tl) detector. The effective solid angle ratio calculation is obtained from dividing the effective solid angle for the cylindrical source, defined in eq. (11), over the effective solid angle of reference, axial point source placed at a distance 50 cm [16]. These values listed in tab. 2. Figures 7 and 8 show the variation of full energy peak efficiency using cylindrical sources (V1and V2) and

Table 2. The values of the effective solid angle ratio

Nuclide	Energy [keV]	$\frac{\Omega_{V1}}{\Omega_{point}}$	$\frac{\Omega_{V2}}{\Omega_{point}}$
^{241}Am	59.53	208.805	63.647
^{133}Ba	80.99	203.677	63.544
^{152}Eu	121.78	188.825	60.895
^{152}Eu	244.69	181.761	60.629
^{152}Eu	344.28	169.259	57.501
^{137}Cs	661.66	155.388	52.666
^{152}Eu	778.9	156.701	52.592
^{152}Eu	964.13	151.189	49.706
^{60}Co	1173.23	145.854	46.621
^{60}Co	1332.5	141.156	44.063
^{152}Eu	1408.01	136.793	42.203

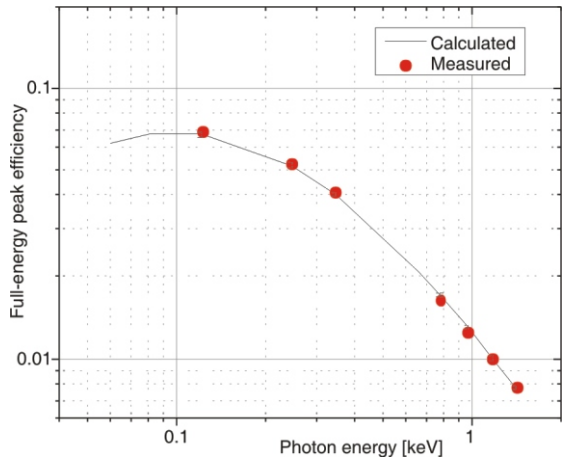

Figure 7. The variation of full energy peak efficiency of NaI (Tl) detector for a cylindrical source V1

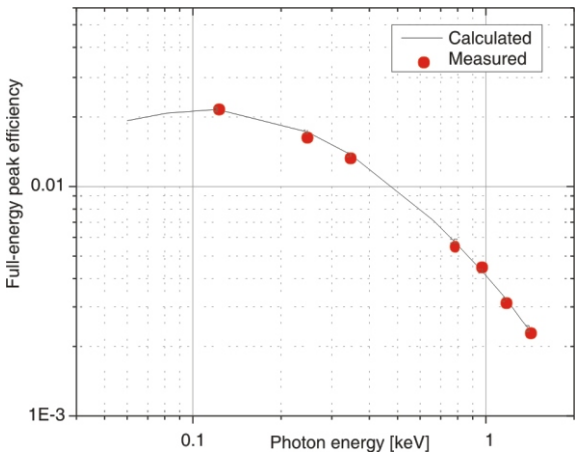

Figure 8. The variation of full energy peak efficiency of NaI (Tl) detector for a cylindrical source V2

based on the reference, axial point source at a distance 50 cm from the detector end cap *vs*. the photon energy. Error bars are included in the figures, but they are very small and mostly hidden. The percentage discrepancy between the calculated and the measured efficiencies is given by eq. (43) and show in figs. 9 and 10.

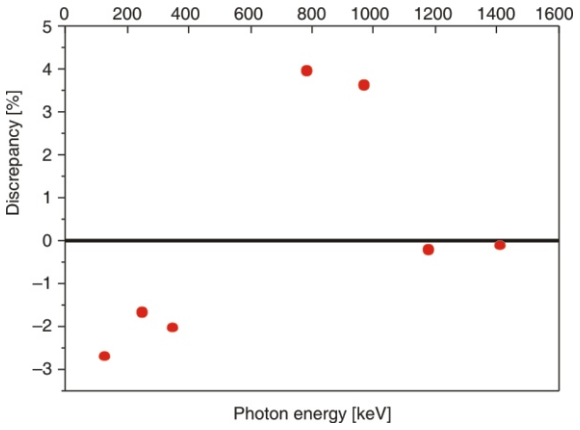

Figure 9. The percentage error between the measured and calculated full energy peak efficiency for V1

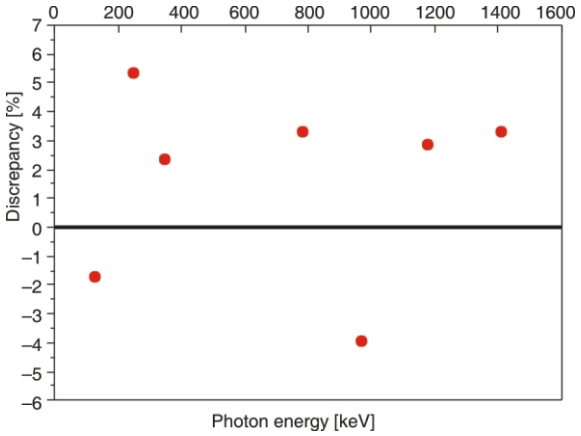

Figure 10. The percentage error between the measured and calculated full energy peak efficiency for V2

$$\text{Discrepancy} \quad \frac{\varepsilon_{\text{calculated}} \quad \varepsilon_{\text{measured}}}{\varepsilon_{\text{measured}}} \; 100\ [\%] \quad (43)$$

where $\varepsilon_{\text{calculated}}$ and $\varepsilon_{\text{measured}}$ are calculated and the measured efficiencies, respectively. The discrepancies were found to be less than 6 % for all energies.

CONCLUSIONS

The full energy peak efficiency was calculated in the energy range from 59.52 keV to 1408 keV by using simple and direct mathematical expressions companion with efficiency transfer technique. The present work is used for calibrating the detectors when there is no available standard source. Moreover, this work leads to the simplified and accurate method of calculating the activity of standard sources and environmental samples with volumes less than, bigger than or capable that of the detector, where the source is placed with axial shift *vs*. the detector.

ACKNOWLEDGMENT

The author is very much thankful to Dr. Mohamed S. Badawi for his fruitful discussion.

REFERENCES

[1] Huang, T., *et al*., NaI(Tl) Scintillator Read Out with SiPM Array for Gamma Spectrometer, *Nucl. Instr. and Meth. A., 851*(2017), Apr., pp.118-124
[2] Baccouche, S., *et al*., Application of the Monte Carlo Method for the Efficiency Calibration of CsI and NaI Detectors for Gamma-Ray Measurements from Terrestrial Samples, *Appl. Radiat. Isot., 70* (2012), 1, pp. 227-232
[3] Nafee, S. S., *et al*., New Numerical Algorithm Method to Calibrate the HPGe Cylindrical Detectors Using Non-Axial Extended Source Geometries, *Appl. Radiat. Isot., 68* (2010), 9, pp. 1809-1815
[4] Lippert, J., Detector-Efficiency Calculation Based on Point-Source Measurement, *Appl. Radiat. Isot., 34* (1983), 8, pp. 1097-1103
[5] Nakamura, T., Matrix Effects in the Activity Measurement of Environmental Samples-Implementation of Specific Corrections in a Gamma-Ray Spectrometry Analysis Program, *Applied Radiation and Isotopes, 48* (1997), 1, pp. 59-69
[6] Selim, Y. S., *et al.*, Analytical Calculation of the Efficiencies of Gamma Scintillators. Part I: Total Efficiency of Coaxial Disk Sources, *Radiat. Phys. Chem., 53* (1998), 6, pp. 589-592
[7] Abbas, M. I., *et al.*, HPGe Detector Photopeak Efficiency Calculation Including Self-Absorption and Coincidence Corrections for Cylindrical Sources Using Compact Analytical Expressions, *Radiat. Phys. Chem., 61* (2001), 3-6, pp. 429-431
[8] Hamzawy, A., Simple Analytical Formula to Calculate γ-Ray Cylindrical Detectors Efficiencies, *Nucl. Instr. and Meth., A 624* (2010), 1, pp. 125-129
[9] Abbas, M. I., *et al*., Full-Energy Peak Efficiency of *Asymmetrical Polyhedron Germanium Detector, Nucl Technol Radiat., 33* (2018), 2, pp. 150-158
[10] Moens, L.*, et al*., Calculation of the Absolute Peak Efficiency of Gamma-Ray Detectors for Different Counting Geometries, *Nucl. Instr. and Meth., 187* (1981), 2-3, pp. 451-472
[11] Thabet, A. A., *et al*., Experimental Verification of Gamma-Efficiency Calculations For Scintillation Detectors In Angle 4 Software, *Nucl Technol Radiat, 30* (2015), 1, pp. 35-46
[12] Gouda, M. M., *et al*., Mathematical Method to Calculate Full-Energy Peak Efficiency of Detectors Based on Transfer Technique, *Indi. Jour. Phys., 90* (2016), 2, pp. 201-210
[13] Mihaljević, N., *et al*., A Mathematical Model of Semiconductor Detector Gamma-Efficiency Calibration for Rectangular Cuboid (Brick-Shape) Sources, *Nucl Technol Radiat, 33* (2018), 2, pp. 139-149
[14] Abbas, M. I., *et al*., Calibration of Cylindrical Detectors Using a Simplified Theoretical Approach, *Appl. Radiat. Isot., 64* (2006), 9, pp. 1057-1064
[15] Badawi, M. S., *et al*., New Algorithm for Studying the Effect of Self-Attenuation Factor on the Efficiency of γ-Rays Detectors, *Nucl. Instrum. Meth. A., 696* (2012), Sept., pp. 164-170
[16] Gouda, M. M., *et al*., Calculation of NaI(Tl) Detector Full-Energy Peak Efficiency Using the Efficiency Transfer Method For Small Radioactive Cylindrical Sources, *Nucl Technol Radiat, 31* (2016), 2, pp. 150-158
[17] El-Khatib, A. M., *et al*., Calculation of the Full-Energy Peak Efficiency of NaI(Tl) Detector Using the Efficiency Transfer Method For Large Radioactive Cylindrical Sources, *Chin. Jour. Phys., 54* (2016), 4, pp. 592-606
[18] Hendee, W. R., Ritenour, E. R., *Medical Imaging Physics*, 4th Edition, John, Wiley, New York, USA, 2002

Received on July 8, 2019
Accepted on September 19, 2019

Мона М. ГОУДА

КАЛИБРАЦИЈА ЦИЛИНДРИЧНОГ NaI(Tl) ДЕТЕКТОРА ПРИМЕНОМ АКСИЈАЛНО ПОМЕРАНИХ ЦИЛИНДРИЧНИХ РАДИОАКТИВНИХ ИЗВОРА

У овом раду израчуната је ефикасност на енергији фото-пика пуне енергије NaI детектора новим теоретским приступом користећи неаксијалне цилиндричне изворе. Овај приступ зависи од методе трансфера ефикасности и аналитичких прорачуна средње дужине пута гама фотона од унутрашњости извора до детекторског система. Измерене ефикасности добијене су употребом течног цилиндричног радиоактивног извора ^{152}Eu запремина 25 ml и 400 ml. Поређење израчунатих ефикасности са измереним показује добру сагласност чиме се омогућава потврђивање описаног поступка.

Кључне речи: ефикасност на енергији фото-пика пуне енергије, цилиндрични извор, средња дужина пута, ефективни однос просторног угла, метода трансфера ефикасности